JAAS

Journal of Analytical Atomic Spectrometry

Accepted Manuscript

This article can be cited before page numbers have been issued, to do this please use: C. Sánchez, R. Sánchez, L. P. Charles-Philippe and J. Todoli Torro, *J. Anal. At. Spectrom.*, 2021, DOI: 10.1039/D1JA00134E.

View Article Online
DOI: 10.1039/D1JA00134E

ICP-MS spatial profiles in presence of ethanol and their application for the analysis of ethanol containing samples

Carlos Sánchez,[a,†,*] Raquel Sánchez,[a] Charles-Philippe Lienemann,[b] José-Luis Todolí[a]

[a]Department of Analytical Chemistry, Nutrition and Food Sciences, University of Alicante. P.O. Box 99, 03080, Alicante, Spain.

[b]IFP Energies Nouvelles, Rond-point de l'échangeur de Solaize, BP 3, F-69360 Solaize, France.

[†]Current address: Agilent Technologies Spain, World Trade Center, South Building 5th floor, 08039, Barcelona, Spain.

Abstract

A total sample consumption system (hTISIS) was used for the first time to evaluate the plasma spatial ion profile for ethanolic samples in ICP-MS. The effects of the extraction lens voltages, the inner diameter of the torch injector, the plasma sampled zone, spray chamber temperature and nebulizer and high matrix introduction gas flow rates on the plasma ion cloud distribution were systematically studied. Regarding the minimization of matrix effects caused by ethanolic matrices, it was found that extraction lenses voltages and the injector inner diameter played a key role when the hTISIS was set at 300 ^{o}C. Under these conditions, the aerosol transport interferences were eliminated. The combination of the widest injector (2.5 mm id) with a 5V extra lens voltage allowed the mitigation of the matrix effects. Moreover, it was observed that for a 2.5 mm id injector, the interferences could be mitigated irrespectively of the plasma sampled volume. Meanwhile, for narrower injectors, it was necessary to carefully select the plasma sampled zone. Finally, the accurate determination of As, Cd, Co, Cr, Cu, Fe, Mn, Ni, Rb, Sr, V and Zn in bioethanol and beverages (wine, whiskey, gyn, vodka, rum and apple liqueur) was performed under optimum experimental conditions.

View Article Online
DOI: 10.1039/D1JA00134E

Introduction

Different methods have been developed for the analysis of ethanolic matrices using ICP techniques. An application field is the determination of the metal content in spirit beverages. The sources of metals in beverages can be very different including raw materials (soil, water, grape…), growing practices (fertilization, pesticide use in phytosanitary treatments), production procedure, storage and adulteration.[1] Elemental composition provides relevant information on the quality of alcohol containing beverages, their origin and preservation.[1,2,3,4,5,6,7]

The development of new analysis methods to determine metals and metalloids in bioethanol is being recently developed due to the expanded use of biofuels.[8,9,10,11,12] The determination of metals and metalloids in this kind of samples has several difficulties: (i) the metal content is usually low (i.e., sub-ppb levels); (ii) reference materials are not commercially available; and, (iii) bioethanol samples may contain up to 300 different organic compounds together with water at the percentage level [13], hence leading to potential matrix effects.[8,9,14]

Several techniques and methodologies have been successfully used to carry out the quantification of metals in the so-called ethanol fuel (i.e., an ethanol – gasoline blend).[8] However, a limited number of studies have been focused on the determination of metals in pure bioethanol.[8,9,14,15] Various analytical techniques have been proposed to determine metals in ethanol matrices. Among them, ICP techniques (ICP-OES and, specially, ICP-MS) have been deeply studied due to their low limits of quantification and multielemental capabilities. In general terms, ICP

techniques have been optimized to reach the maximum sensitivity. However, ICP techniques suffer from non-spectral interferences caused by the ethanolic matrices that degrade the accuracy of the determinations and experimental conditions need to be optimized to develop accurate methods based on this technique. Non-spectral interferences, related to sample introduction, atomization, ionization, ion extraction and transport, could be overcome by using sample dilution,[16,17] matrix matching[17,18] matrix decomposition[19] or internal standardization.[17,20] However, all these procedures present some drawbacks such as loss in sensitivity, degradation of limits of detection, time consumption, potential sample contamination, or the lack of appropriate elements to be used as internal standard.

Recently, an alternative sample introduction system has been proposed to remove the matrix effects caused by volatility effect and more specifically by ethanol. The use of the high temperature torch integrated sample introduction system (hTISIS) has been reported as a possibility to remove the matrix effects in the analysis of non-diluted wine and 1:1 diluted bioethanol samples.[7,14,21] Additional advantages of the hTISIS over conventional sample introduction systems included the shortening of analysis time, the suitability for the routine analysis and the improvement of sensitivity and limits of detection. For example, limits of detection for the analysis of non-diluted wine samples by using the hTISIS were from 2 to 40 times lower than those found for microwave digested samples and analysed using a conventional sample introduction system.[7] Thus, by setting the hTISIS temperature at 400 ^{o}C, ICP-OES sensitivities for water and ethanol did not differ significantly.[14] Under these circumstances, the analyte transport

efficiency was close to 100% regardless of the matrix considered[14] and ICP-MS non-spectral interferences caused by a 50% ethanol concentration were removed.[21] Besides heating the spray chamber, it was necessary to modify the torch-interface alignment in order to fully remove the matrix effects.[21] These results suggest that the spatial distribution should be fully characterized in order to understand the role of ethanol in terms of the ions migration within the plasma. Thus, interferences produced by ethanol and other organic matrices in ICP-MS could be better understood, hence opening a possible way to overcome them.

In the past 25 years, the spatial distribution of the analytes in the plasma has been deeply characterized in ICP-MS.[22] This is a very important point precluding the sensitivity of the analytes, the signal of doubly-charged ions, oxides and the background ions.[22] It has been noticed that the radial profiles, which can provide valuable insight into the dominating ionization mechanism and the extent of the analytes diffusion in the plasma, show a centered plasma axis bell-shaped profile.[22,23,24] Besides, the ion spatial distribution along the z axis, which provides information about the energy and the time necessary to generate ions, depends on the operating conditions. Thus, for instance, it has been observed that increasing the nebulization flow rate leads to an increase in the optimal sampling depth caused by the shortening in residence time of the analytes inside the plasma.[25,26,27] These observations were confirmed by several studies revealing the effect of the pre-evaporation by means the use of a desolvation system in which the optimal sampling depth was shifted to lower values.[24,28,29] All the studies related with axial and radial plasma profiling revealed that, depending on

the plasma operation conditions, the mass of the measured isotope could[32,30] or could not[26,31,32] affect the ionic plasma profiles. Thus Dziewatkoski *et al.*[30] observed an inverse square root dependence of the diffusion degree with the analyte mass.

Additionally, Aghaei *et al.*[33] carried out a computational simulation which reported that, by enlarging the injector inner diameter, the gas flow exhibited more backward motion inside the torch, which was undesirable for sample transfer to the mass spectrometer. It was also reported that, under a specific set of operating conditions, the higher the injector diameter the lower the speed of the tertiary aerosol and, hence, the higher the residence time of the analytes inside the plasma.

Besides operating conditions, the sample matrix may have a direct effect on the degree of the diffusion of analyte ions inside the plasma. These phenomena could exacerbate the matrix effects and should be taken into account in order to increase the accuracy of the determinations. So far, some studies have been carried out in this sense for inorganic matrices such as easily ionized elements.[34] However, to the best of the authors knowledge, there are not previous attempts to characterize the spatial behaviour of analyte and background ions in the plasma as a function of the ethanol content.

Another influential parameter in ICP-MS signals is the ion transmission energy. This parameter, defined as the ability of collecting and transmitting the maximum fraction of ions from the plasma to the mass spectrometer, depends on the diameter of the sampler and skimmer and the extraction lenses potentials.[33,35,36,37]

View Article Online
DOI: 10.1039/D1JA00134E

The aim of the present work was thus to evaluate the ion cloud distribution by means of axial and radial spatial profiling for different aqueous solutions containing variable concentrations of ethanol. The hTISIS,[14,21,38] was employed to evaluate the matrix effects exclusively caused by differences in the ion cloud distribution inside the plasma. In order to further complete the understanding of the phenomena, the impact of the extraction lenses voltage and the injector inner diameter were systematically studied. The final goal of the present work was thus to test the combination of hTISIS-ICP-MS with the main results of the ion cloud distribution studies, as a rapid and direct way for performing accurate multielemental determination in ethanol matrix samples: alcohol containing beverages and bioethanol.

Experimental

Standards. Aqueous standards containing from 0 to 50% of ethanol were prepared using ultrapure water (R < 18.2 MΩ) obtained with a Millipore water purification system (El Paso, TX, USA) and analytical grade ethanol 96% (Panreac, Barcelona, Spain). All these synthetic standards were spiked with 500 ng mL^{-1} of the analytes present in the multielemental Merck IV ICP standard (Merck, Darmstadt, Germany) and Cerium (Merck, Darmstadt, Germany). A series of blanks containing the same percentage of ethanol and water were prepared. All the blanks and standards were filtered with a 0.45 µm Nylon filter pore size (Filabet, Barcelona, Spain).

A series of aqueous standards containing 25% of ethanol and concentrations from 1 to 500 ppb of the elements gathered in Table 1 were used to perform the analysis of real samples.

Samples. Twenty bioethanol, wines and spirit beverages real samples with different ethanol concentrations, ranging from 10% to 50%, were analyzed. Six bioethanol samples (diluted 1:1 with ultrapure water), three whiskey samples, three gyn samples, two vodka samples, two white wines, two red wines, one rum sample and one apple liqueur sample.

Instrumentation. An Agilent Technologies 7700x ICP-MS spectrometer (Santa Clara, California, USA) equipped with a high matrix introduction system (HMI) and a collision cell with He as a collision gas was employed to take the ionic intensities of the analytes shown in Table 1. The main operating conditions are also gathered in Table 1.

The introduction system was a glass pneumatic concentric nebulizer, TR-50-C0.5 (Meinhard Glass Products, Santa Ana, USA) and a hTISIS system equipped with a 9 cm^3 single-pass spray chamber. Strictly speaking the nebulizer chosen was not considered as a 'micro nebulizer', nevertheless it was able to provide satisfactory analytical figures of merit when liquid flow rates on the order of tens of microliters per minute were selected. The solutions were delivered in continuous sample aspiration mode to the nebulizer by means of a peristaltic pump Perimax 16 antiplus, (Spetec GmbH, Erding, Germany) and a 0.19-mm id flared end PVC-based tubing (Glass Expansion, Melbourne, Australia).

View Article Online
DOI: 10.1039/D1JA00134E

Three different torches, that incorporating different injector inner diameters, were evaluated in the present work: (*i*) 2.5 mm id (Ref. G3280-80001, Agilent, California, USA); (*ii*) 1.5 mm id (Ref. G3280-80080, Agilent, California, USA); and, (*iii*) 1.0 mm id (Ref. G3280-80081, Agilent, California, USA). The nebulizer and dilution gas flow rates (see Table 1) were not modified for the three different injectors in order to avoid differences in terms of transport efficiency. Under these conditions, the mass of matrix and ions reaching the torch were virtually the same for the three different injectors.

Table 1. Operating conditions of the ICP-MS system.

Plasma	
Ar flow rates/L min^{-1}	Plasma gas: 15.0 Auxiliary gas: 0.9 Nebulizer gas: 0.4 Dilution gas (HMI): 0.56
RF power/W	1600
Sampling depth (axial pos.)/mm	3 to 20
hTISIS	
Liquid flow rate/ µL min^{-1}	25
Number of replicates	5
Integration mode	Spectrum
Integration time/s	0.3
Sweeps per replicate	100

View Article Online
DOI: 10.1039/D1JA00134E

Collision cell	
He flow rate/mL min^{-1}	4.3
OctP Bias/V	-18
Oct RF/V	200
Energy discrimination/V	3.0
Lenses	
Extract 1/V	-30 to 10 (*)
Extract 2/V	-250 to -150 (*)
Omega bias/V	-85
Omega lens/V	7.0
Cell entrance/V	-40
Cell exit/V	-70
Deflect/V	-0.6
Plate Bias/V	-60
Q-Pole	
Mass gain	132
Mass offset	124
Axis Gain	1.0115
Axis Offset	0.10
QP Bias/V	-15.0
Axial and radial torch position	
Sampling depth/mm	3 to 25
Vertical position/mm	-2 to 2

View Article Online
DOI: 10.1039/D1JA00134E

Horizontal position/mm		0.0	
Measured isotopes			
^{9}Be	^{51}V	^{52}Cr	^{55}Mn
^{56}Fe	^{59}Co	^{60}Ni	^{63}Cu ^{65}Cu
^{66}Zn	$^{140}Ce^{++}$	^{75}As	^{85}Rb
^{88}Sr	^{111}Cd	^{140}Ce	$^{140}Ce^{16}O$

* Analysis of real samples carried out under optimum conditions of extraction lenses. Extract1 set to 0 V and Extract2 set at -200V.

Results and discussion

ICP-MS analytical ionic intensity

In order to evaluate the effect of the ion cloud distribution the sensitivity and matrix effects, the ICP-MS signals were measured for the elements listed in Table 1. Similar results were found for all elements, independently of their ionization potential (see in Figure S1). Therefore, with the aim to clarify the information discussed through this section, only the results for manganese have been discussed.

Effect of the extraction lens applied voltage. The ICP-MS Agilent 7700x spectrometer was equipped with an interface consisting of two cones (sampling cone and skimmer cone) and four different lenses (extraction-omega lens assembly). The first and second extraction lenses, so-called extract 1 and extract 2 respectively, are used to focus the ions stream after the supersonic expansion. The extract 1 can be modified from -200 to 10 V. In aqueous applications, this lens is commonly set at 0 V to prevent surface

contamination and provide the instrument with better long-time stability. The extract 2 can be modified from -250 to 10V and it is commonly set at between -200 and -100V. This lens is responsible for accelerating the ion cloud after the supersonic expansion. After these lenses, the ions stream passes through the omega lens and omega bias, which separate the ions positively charged from negative and neutral species to prevent their entrance into the octopole.

Figure 1 shows the results obtained for the 25% ethanol solution. It was experimentally verified that the ion transmission efficiency depended primarily on the voltage applied to the extraction lens 1. Therefore, this variable was systematically evaluated in terms of analytical sensitivity and its effect depended strongly on the injector used (Figure 1.a). Thus, when a 2.5 mm inner diameter injector was used, the sensitivity peaked at 5V for all the matrices. This trend was observed regardless the chamber temperature. In contrast, for the 1.0 mm id injector, changes in the extract 1 lens voltage affected much less the sensitivity. This was likely due to an increased ions kinetic energy and, hence, it was not necessary to apply a high voltage to achieve a high ions transmission efficiency. Meanwhile, the use of the 1.5 mm id injector presented an intermediate situation. In this case, plain water solutions (see section “Matrix effects caused by ethanol”) appeared to be more affected by this variable in terms of ionic signal, especially at high hTISIS heating temperature.

Obviously, the injector inner diameter played a critical role from the point of view of sensitivity and variables effect. Comparatively speaking, sensitivity was much lower for the 1.0 mm id injector than for the wider diameter injectors (Figure 1.a). This result was attributed to the shortening in the plasma residence time caused by the increase in the

View Article Online
DOI: 10.1039/D1JA00134E

aerosol velocity as the injector diameter decreased. The sensitivity was maximum for the 1.5 mm id injector that apparently represented a compromise situation between ions kinetic energy (sampling efficiency) and aerosol velocity (plasma residence time). The former point dictated the ion formation efficiency whereas the second one did the ion sampling efficiency. The nebulizer and dilution/make up gas flow rates were kept constant in order to achieve a complete penetration of the aerosol into the plasma, simultaneously, keeping constant the sample transport efficiency through the spray chamber.

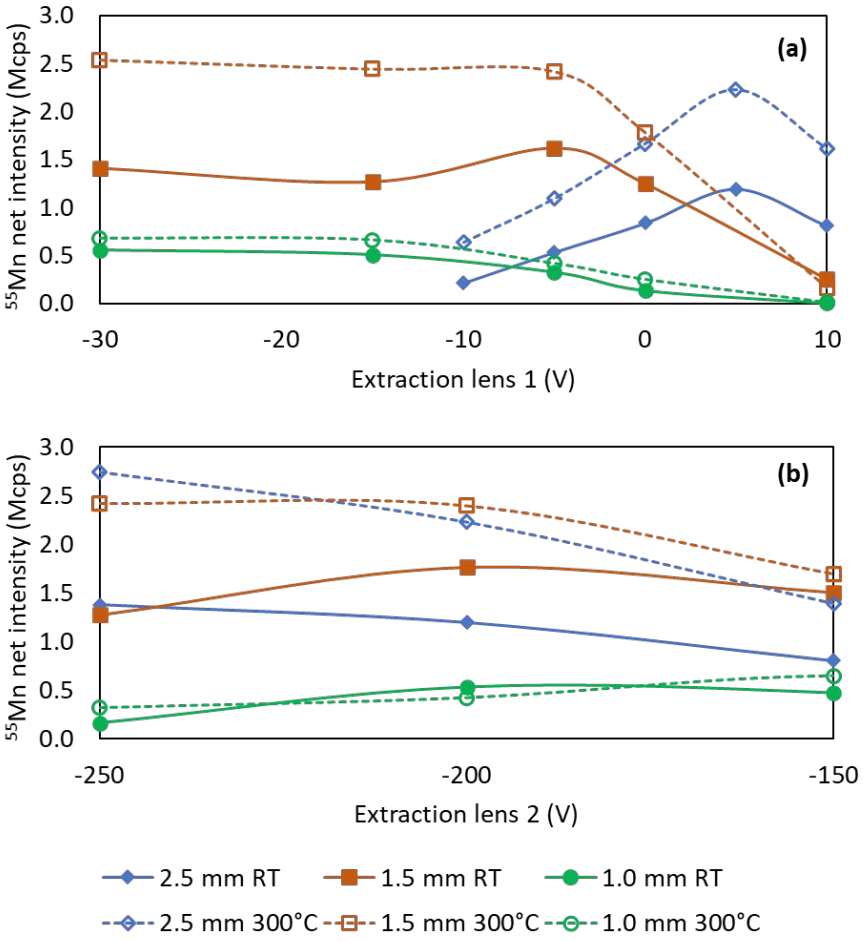

Figure 1. Effect of (a) extraction lens 1 (extraction lens 2 at -200V) and (b) extraction lens 2 (extraction lens 1 at 0V) on ^{55}Mn intensity for the three injectors tested in the present

work. hTISIS temperatures: RT and 300°C. Matrix: 25% ethanol. Radial position: 0.0 mm. Axial position: 10.0 mm. Rest of parameters: See Table 1.

Summarizing, the optimum extract lens voltage in terms of sensitivity was roughly +5V for the 2.5 mm id diameter injector and from 0 to -5V for the two remaining studied cases. Apparently, the use of narrower injectors led to a decrease in the optimum extract voltage in agreement with the increase in the ion kinetic energy.

An alternative study was performed in order to verify the effect of the extract 2 lens voltage in terms of both sensitivity and ethanol matrix effects. Clearly, the effect of this variable was much lower than that for the extract lens 1 voltage. The torch equipped with the 1.0 mm injector showed a smooth maximum in sensitivity between -200 V and -150 V. This maximum was moved to more negative values for the 1.5 mm id injector whereas the sensitivity for 2.5 mm decreased as the extract 2 increased. It was also remarkable that matrix effects were not removed by merely modifying the extract 2 lens applied voltage (data not shown).

Effect of the spray chamber temperature. The influence of the chamber temperature on the axial signal profiles was studied systematically for the three different injectors. Figure 2 shows the results obtained using 1.0 mm id injector, which provided the most significant differences. Two matrices were tested and four hTISIS temperatures were evaluated: 20 (Room Temperature), 100, 200 and 300 ^{o}C. In general terms, it may be stated that optimum sensitivity was higher when heating the chamber than at room temperature. The obvious reason was that the analyte mass delivered to the plasma became higher at the highest evaluated temperature.

View Article Online
DOI: 10.1039/D1JA00134E

Additional observations were made from Figures 1 and 2: *(i)* it was verified that an increase in the hTISIS temperature did not cause significant modifications in the curves obtained when varied the extract lens voltage for all-three injectors evaluated (Figure 1); *(ii)* an increase in the chamber temperature led to a shift in the maximum of the curves upstream the plasma. This effect was injector dependent being more significant when the 1 mm id injector tube was set (Figure 2.a and Figure 2.c); *(iii)* somewhat wider radial signal profiles were obtained when the chamber temperature was increased up to 300 ^{o}C (see Figure 2). This latter observation suggested that, as solvent was evaporated prior to its introduction into the plasma, ions were generated closer to the plasma base at high than at low chamber temperatures. Consequently, there was a higher likelihood for ions transversal diffusion when heating the chamber. To explain the effect of the temperature on the profiles, the plasma charge effects (ion repulsion) had to be taken into account. The increase in hTISIS temperature boosted the transport efficiency of analyte and matrix. Under these circumstances, the different population of matrix ions in the plasma could modify the signal profiles through repulsions. It had also to be considered that the extent of the space-charge effects in the ICP-MS interface could be different depending on the plasma sampled zone and the hTISIS temperature. These latter effects could be the subject of further studies.

On this subject, it was figured out that water provided sharper and higher axial and radial profiles than ethanol solutions when the chamber temperature was set above 100 ^{o}C. In addition, it was found that, at low sampling depth values, the signal for ethanol samples was higher than for plain water. A cross-over point was localized at 5-7 mm axial position above which, water provided higher ionic intensities than ethanol solutions. This might suggest that, on the one hand, ethanol promoted the analyte

ionization at locations closer to the plasma base than in the case of water standards, and, on the other, in the case of ethanol solutions, analyte diffused transversally. In order to verify the latter point, radial profiles were obtained (Figure 2.b and Figure 2.d). As expected, the profiles for ethanol:water mixtures were wider than those plotted in absence of this alcohol. According to our forecast, this effect became more significant as the chamber temperature went up, because a fraction of the energy required for the plasma to evaporate the solvent was supplied to the aerosol in the spray chamber.

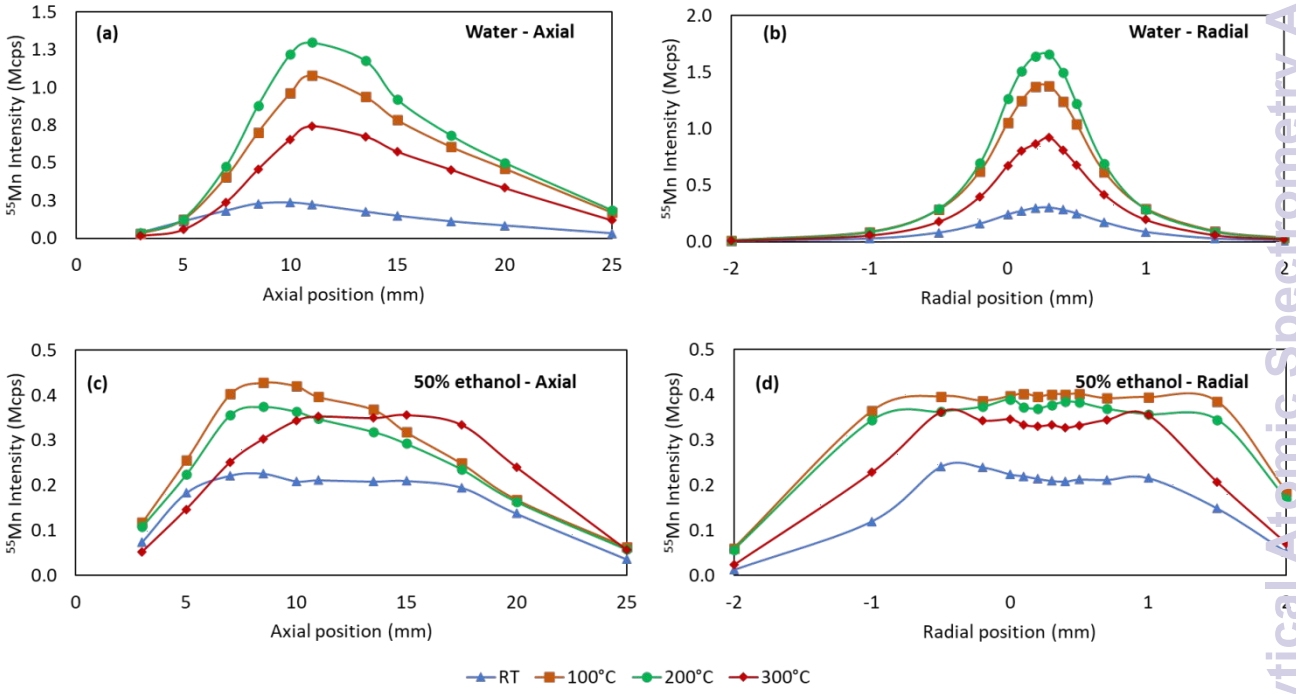

Figure 2. Effect of hTISIS temperature on axial (a, c) and radial (b, d) analyte profiles for water (a, b) and 50% ethanol (c, d) matrices. Analyte: ^{55}Mn. Injector id: 1.0 mm. Ref. axial position: 10 mm. Ref. radial position: 0.0 mm. Rest of parameters: optimized (Table 1).

View Article Online
DOI: 10.1039/D1JA00134E

Effect of the plasma sampled zone. The plasma position with respect to the sampling cone of the ICP-MS interface was varied and the ionic intensity taken for two matrices (water and 50% EtOH) and the hTISIS at 300 ^{o}C. Data were taken for the three injectors studied. Figure 3 shows the effect of the plasma horizontal (*i.e.*, axial) and vertical position (*i.e.,* radial) on sensitivity. The role of the injector tube was clearly evidenced from Figure 3.a, because the lower the id diameter, the higher the optimum axial position. This expected trend was due to a shift of the analyte ionization zone downstream the plasma as the aerosol residence time shortened (*i.e.*, higher aerosol velocity for the 1 mm id injector than for the 2.5 mm one). It was noticed that the optimum sensitivity for the 2.5 mm id injector was higher than for the two additional torches tested, thus revealing the benefit of a long residence time. This is not the only parameter that could be affected, but also the plasma ionization characteristics could play an important role. In the present work, the plasma thermal state was monitored through the determination of the oxide ratio (CeO^+/Ce^+) and ^{36}Ar profiles (Figure 6) for the different matrices and injector inner diameters used.

When considered the plasma radial position (Figure 3.b), it was clearly observed that, for all the assayed situations, a maximum in signal was found at an area slightly off plasma axis regardless the injector id. Nevertheless, this variable played a significant role from the point of view of profile width. This was especially evidenced when compared the profiles obtained in the case of the 1 mm id injector against those found when the 2.5 mm id injector was studied.

Taking into consideration the sample composition, it is worth to mention that the width and the shape of the radial profiles were similar for both matrices when the 2.5 mm injector was adapted. The 1.5 mm injector, in turn, afforded results strongly

dependent on the chamber temperature and ethanol content. Thus, at RT the profile for 50% ethanol reached a plateau from -0.5 mm to 1 mm. However, the profile for water showed a maximum between 0 mm and 0.5 mm. Additionally, the profile for 50% ethanol was wider than those for water and 25% ethanol (data not shown). As a consequence, the signal for 25% ethanol in the central channel of the plasma-interface was higher than the obtained for 50% ethanol. When the temperature increased up to 300 ^{o}C, the plateau for ethanol was extended from -1.0 mm to 1 mm (Figure 3.b). These facts could be related with the ionic dispersion in the plasma (spatial effects) as a function of the matrix.

Besides, the injector diameter plays an important role because the modification of this parameter causes changes in the aerosol velocity at the plasma base. This trend was evidenced for the 1.0 mm injector where the signal for ethanolic solutions reached a plateau when the hTISIS was heated at 300 ^{o}C, whereas water showed a maximum at 0.2 mm. From -0.5 mm to 0.7 mm, water showed higher signals than ethanolic solutions (Figure 3.b).

It is noteworthy that the sensitivity improvement factor incorporated by the hTISIS at high temperatures as compared to RT decreased with the injector diameter. For example, for a 50% ethanol standard, the improvement factors provided by hTISIS at 300^{o}C as compared to room temperature (for ^{55}Mn) were approximately 3.5, 1.3 and 1.2 for 2.5, 1.5 and 1.0 mm diameter injectors, respectively. When plain water standard was injected, the respective factors were 7.2, 3.0 and 2.8. This may be directly related with the analyte residence time inside the plasma. It should be noted that optimum temperature in terms of transport efficiency is, as expected, above the boiling point of the solvent.

View Article Online
DOI: 10.1039/D1JA00134E

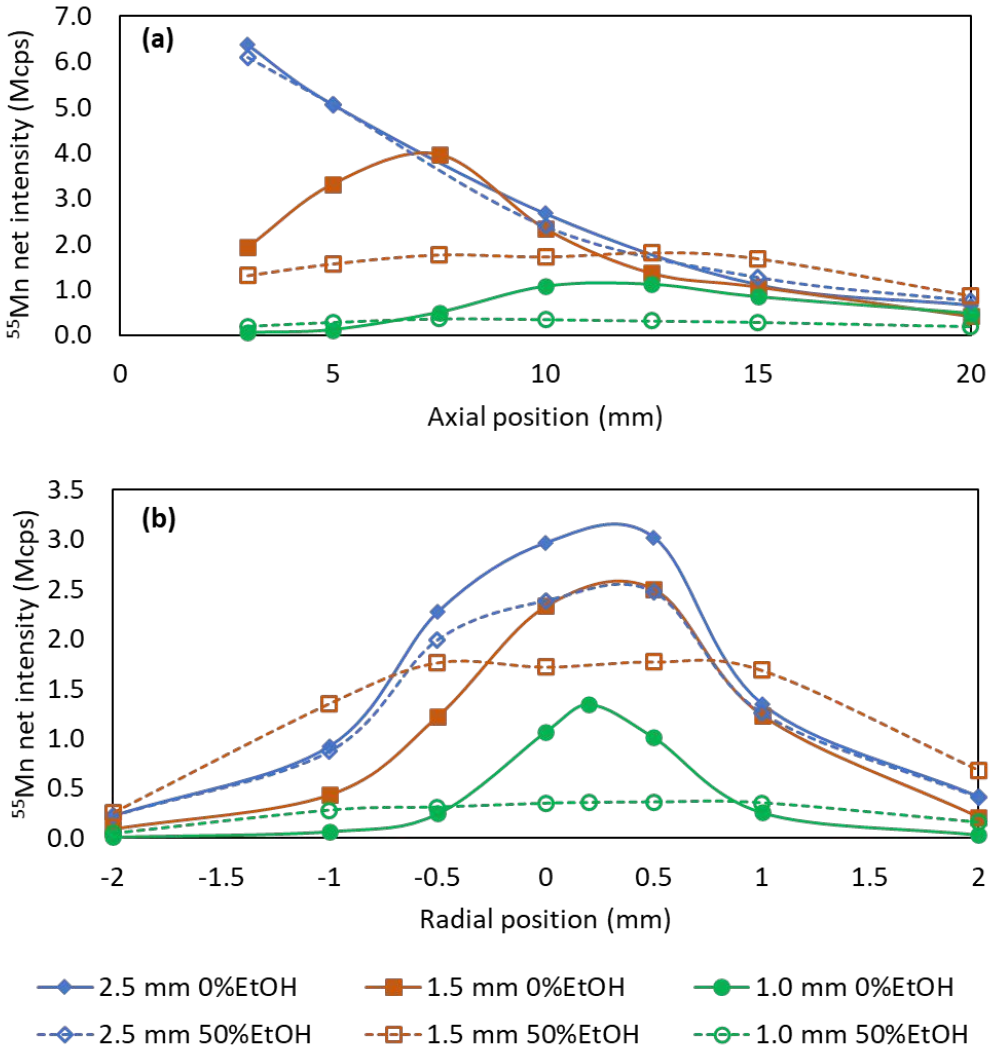

Figure 3. Effect of injector inner diameter and matrix composition (ethanol concentration) on axial (a) and radial (b) analyte profiles. Analyte: ^{55}Mn. hTISIS temperature: 300°C. Ref. axial position: 10 mm. Ref. radial position: 0.0 mm. Rest of parameters: optimized (Table 1).

Effect of the nebulizer gas, Q_g, and HMI flow rates. The spectrometer used has the option of adding an argon stream at the exit of the spray chamber via a "tee" joint. Thus the influence of the nebulizer gas flow rate on the ionic intensity was studied in two

different ways: *(i)* increasing the nebulizer gas flow rate and keeping constant the HMI flow rate at 0.56 L min^{-1}; and, *(ii)* keeping constant the central gas flow rate. According to preliminary tests, 0.96 L min^{-1} corresponded to the optimum central gas flow rate in terms of sensitivity. Therefore, in the situation *(ii)*, both the nebulizer and HMI gas flow rates were modified so as to keep their sum at 0.96 L min^{-1}.

Figure 4 shows representative axial profiles obtained for the 25% ethanol:water solution. The selected data correspond to the hTISIS operated at 300 ^{o}C and 2.5 mm injector inner diameter. The obtained curves peaked at very different Q_g values when the HMI flow rate was kept constant and the central one was increased. This fact moved upstream the optimum sampling depth as a longer analyte – plasma interaction was required to efficiently generate ions. In the case of 25% ethanol sample, by increasing Q_g, two phenomena were produced: first primary aerosols became finer; and, second, the aerosol heating efficiency decreased as its residence time inside the hTISIS shortened. The last point may cause a decrease in the analyte transport efficiency and/or in the solvent evaporation degree. As a result, an increase in the optimum sampling depth would be expected. According to the obtained results, this effect appeared to be more significant for water than for a more volatile matrix containing 50% ethanol. Moreover, for water samples, this effect was exacerbated as the injector id went down. Nevertheless, when worked with ethanol solutions, the opposite trend was observed.

The data found when both Q_g and the sheathing gas flow rate were varied to keep constant the central flow rate indicated that the signal profiles were virtually the same regardless of the matrix and isotope considered. It should be note that, although the

View Article Online
DOI: 10.1039/D1JA00134E

profiles were similar for different matrices, the net intensities were different for the matrices studied, depending also on the plasma sampled zone.

Radial profiles were also obtained for all the matrices considered. The results indicated that for a 100% water standard, the profiles did not appreciably change when the total central gas flow rate was kept constant. Nonetheless, when the increase in Q_g was not compensated for by lowering the HMI flow rate, the higher the Q_g, the narrower the axial profile width, because the analyte radial diffusion was mitigated as the central flow rate grow. This was especially observed for the 1.5 and 1 mm id injectors. In the case of ethanol solutions, similar trends were found. However, quantitatively speaking, the change in signal radial profiles was much more significant than for water. Thus, for instance, in the case of the 1 mm id injector, the profile widths were around 1.5 mm and higher than 4.0 mm for the highest and lowest Q_g assayed, respectively. As for water, Q_g did not have any remarkable effect when the central gas flow rate was kept constant (*i.e.*, the HMI lowered to compensate for the increase in Q_g).

Finally, the profile width was compared for the matrices under study. Generally speaking, transversal profiles for water were narrower than those recorded when ethanol was present in the sample. Again, this assessment was more significant for the 1.5 and 1.0 mm id injectors. Importantly, these observations confirmed that when ethanol was present in the sample, transversal ions diffusion took place more significantly than for plain water standards.

View Article Online
DOI: 10.1039/D1JA00134E

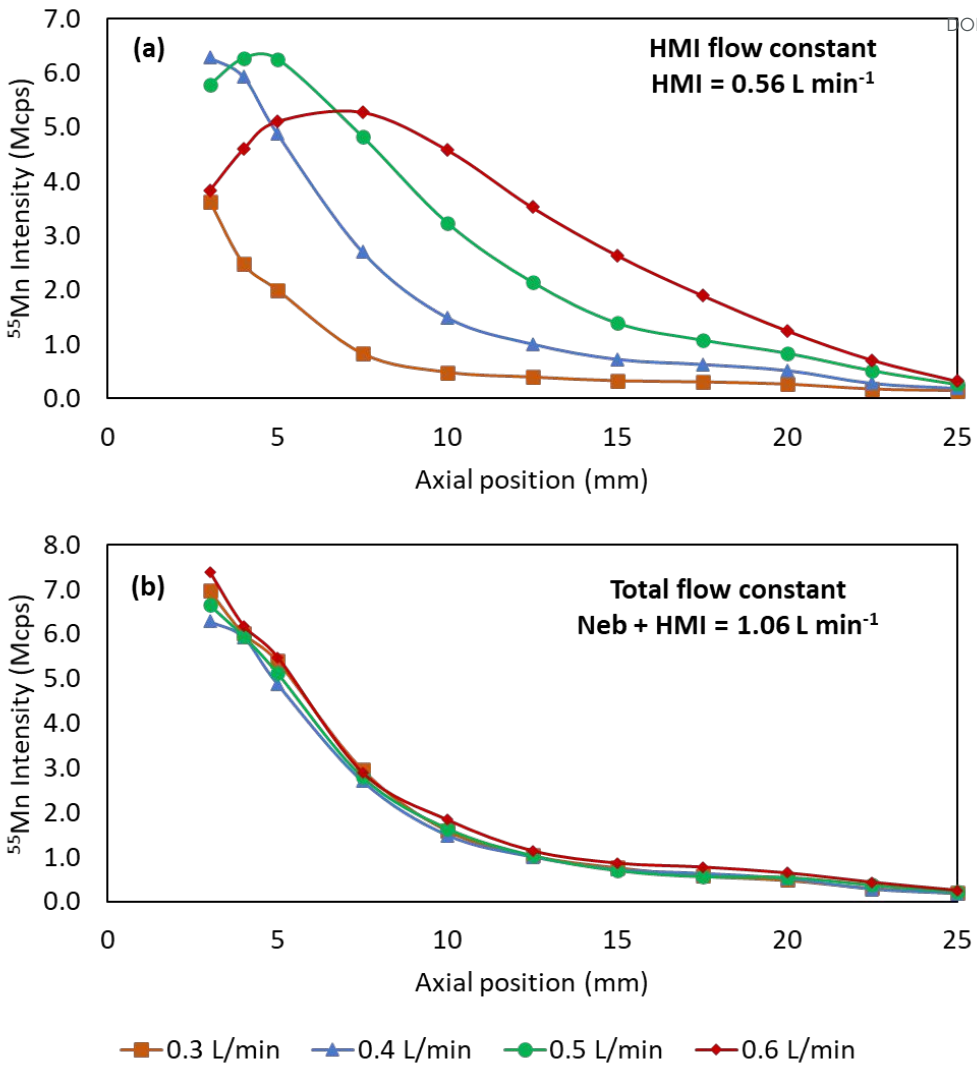

Figure 4. Effect of nebulizer and HMI gas flow rates on analyte axial profiles. (a) HMI constant at 0.56 L min^{-1}, total flow variable and (b) total flow constant at 0.96 L min^{-1}. Analyte: ^{55}Mn. Injector inner diameter: 2.5 mm. hTISIS temperature: 300°C. Matrix: 25% ethanol. Radial position: 0.0 mm. Extract lens 1 and 2, 0 and -200V, respectively. Rest of parameters: Table 1.

Matrix effects caused by ethanol

View Article Online
DOI: 10.1039/D1JA00134E

The interferences caused by ethanol were evaluated by calculating the relative intensity, I_{rel}, defined according to:

$$I_{rel} = \frac{Intensity\ solution\ "i"}{Intensity\ pure\ water} \qquad \text{(Eq. 1)}$$

Equation 1 was useful in order to give information regarding the magnitude of the interference, because the closer the I_{rel} value to 1 the less severe the interferences caused by ethanol are.

Effect of the extraction lens applied voltage. Extract 1 and extract 2 voltages play an important role on matrix effects. When the 2.5 mm id diameter injector was used, signal provided in presence of ethanol was higher than that encountered for plain water. The I_{rel} value ranged from 1.2 to 3.5 depending on the hTISIS temperature and the lens voltage selected. When considering the hTISIS operating at room temperature, the observed matrix effect was attributed to changes in the mass of analyte reaching the plasma as well as to plasma-based phenomena. However, when the chamber temperature was set at 300°C, the aerosol transport-based interferences were removed and changes in sensitivity were entirely due to a modification in the analyte ionization yield and/or transmission.[21] The obtained results were completely different when the 1 mm injector was set. Thus, when the hTISIS was operated at room temperature, I_{rel} was close to 1.5 whereas at 300°C, this parameter took values approaching to 0.5 (*i.e.*, ionic signal was lower for ethanol than for water).

It should be noted that, under some of the assayed conditions, for the hTISIS operated at room temperature, matrix effects caused by ethanol were virtually eliminated. However, under these conditions, it was obvious that the mass of analyte reaching the plasma depends on the ethanol content.[21] Therefore, these situations

View Article Online
DOI: 10.1039/D1JA00134E

corresponded to a rather fictitious removal of matrix effects and they were not reliable. Furthermore, sensitivity was lower when the experiments were performed under these operating conditions.

Finally, it was verified that the hTISIS working at 300°C heating temperature combined with the 2.5 mm id injector and extract voltages close to 5 V provided quite satisfactory results in terms of mitigation of matrix effects. For these experimental conditions, the relative intensity values were in the 0.75-1.25 range. Furthermore, the achieved sensitivity under these circumstances was higher than the obtained at room temperature.

Effect of the plasma sampled zone. Figure 5 plots the I_{rel} values as a function of both radial (Figure 5.a) and vertical position (Figure 5.b) for the three different injectors used in this work. The main conclusion was that the beneficial role of the hTISIS as a system able to remove interferences at high chamber temperatures caused by ethanol depended on the injector used. Clearly, a 2.5 mm id injector favored the mitigation of these effects, because the I_{rel} values were close to 1 regardless of the plasma sampled zone. In contrast, 1.5 and 1 mm id injectors made the extent of the interferences to be strongly dependent on the plasma position with respect to the interface, although it would be possible to find a suitable plasma location to enhance the accuracy of the analytical determinations based on external calibration. Thus, for instance, using the 1.0 mm id injector and setting the sampling depth at 7.5 mm, the sensitivity was virtually the same irrespectively of the ethanol concentration considered. However, the sensitivity under the mentioned conditions was 6-foldlower than that obtained with the hTISIS at 300°C, with the 2.5 mm id injector and moving the torch 1 mm down plasma

View Article Online
DOI: 10.1039/D1JA00134E

axis. Similar comments could be made for the 1.5 mm id injector with the hTISIS operating at room temperature for a sampling depth below 7.5 mm.

Therefore, in order to overcome ethanol effects in ICP-MS with the current setup, the proposed injector id would be similar to that usually established for the analysis of aqueous solutions. This striking conclusion should be due to several reasons: *(i)* very low liquid flow rates are used; *(ii)* the sample introduction system evaporates the totality of the aerosol; and, *(iii)* the spectrometer contains a gas phase dilution accessory.

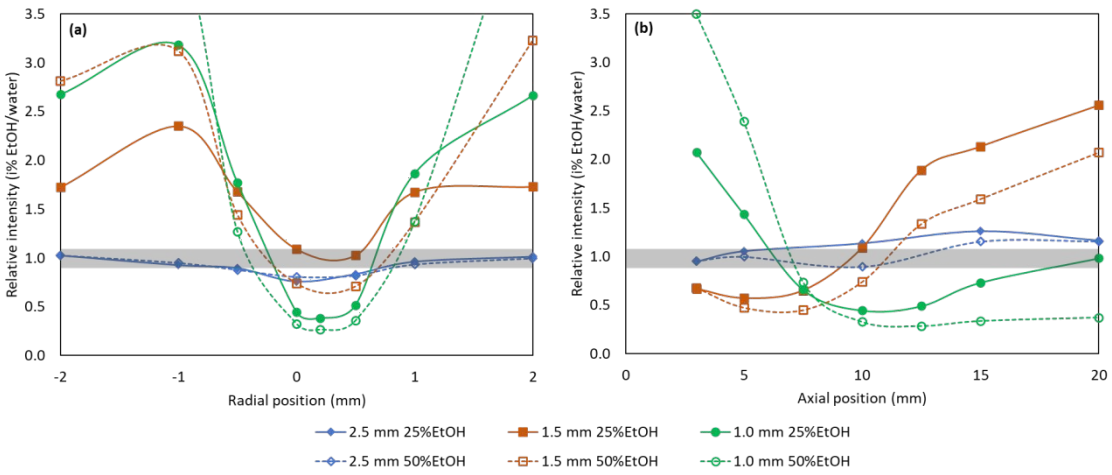

Figure 5. Effect of sampling region on matrix effects for the three injectors studied. Relative intensity of ^{55}Mn. Radial (a) and axial (b) position. hTISIS temperature: 300°C. Ref. axial position: 10 mm. Ref. radial position: 0.0 mm. Extraction lens 1 and 2 at 0V and -200V, respectively. Rest of parameters: Table 1.

Effect on background ions, oxide and doubly charged ions.

Doubly charged ions and oxide ratios could be considered as indicators of the plasma thermal state.[39] The CeO^+ and Ce^{++} ratios were obtained according to equation 2 and 3, respectively.

$$CeO^+(\%) = 100 \cdot \frac{CeO^+}{Ce^+ + Ce^{++} + CeO^+} \quad \text{(Eq. 2)}$$

$$Ce^{++}(\%) = 100 \cdot \frac{Ce^{++}}{Ce^+ + Ce^{++} + CeO^+} \quad \text{(Eq.3)}$$

Effect of the extraction lens applied voltage. The effect of extract 1 and extract 2 voltages on CeO^+ and Ce^{++} ratios was studied. Both extraction lenses did not play an important role on CeO^+ profiles, showing all the matrices and hTISIS temperatures CeO^+ ratios non-dependent on the extraction voltages applied. However, the Ce^{++} ratio was more affected by the extract 1 voltage, providing lower values when positive voltages are applied to this lens. This observation could be associated to the different interaction of doubly charged Ce ions when a positive electric field was applied as compared to the lower repulsion forces suffered by the single charged Ce ions. When extract 2 was modified from -250 to -100V, no effect on the Ce^{++} ratio was observed.

Effect of the plasma sampled zone on background, oxide and doubly charged ions. Figure 6 shows the CeO^+ ratio (Figure 6.a) and $^{36}Ar^+$ (Figure 6.b) axial profiles for the three different injectors used in this work using the hTISIS at room temperature and 300ºC. The CeO^+ ratio decreased with ethanol concentration as the percentage of oxygen in ethanol (34.8%) was lower than in water (88.9%). However, the oxide ratio

View Article Online
DOI: 10.1039/D1JA00134E

not only depends on the composition of the matrix, CeO^+ ratio could be modified by other factors such as robustness of the plasma, injector diameter, sampling depth and mass bias in the interface.

The goal of this part of the work was to compare the trends in terms of plasma stability when using different injector diameters and hTISIS temperatures. Therefore, Figure 6 shows the behavior observed for the 25% ethanol standard. CeO^+ ratio remained below 1% from 20 mm to 10 mm axial position for both hTISIS temperatures, thus indicating that plasma thermal state was optimum and the use of the hTISIS was not causing any plasma thermal degradation. When the distance between the plasma and sampling cone tip was reduced, the oxide ratio increased exponentially, thus indicating that residence time of the ions in the plasma was not long enough to break the chemical bonds created between cerium and oxygen, giving an idea that plasma thermal properties were degraded. However, this increase took place at different axial positions depending on the injector inner diameter. For the 1.0 mm inner diameter torch and hTISIS at room temperature, the CeO^+ ratio increased for axial positions lower than 8 mm, reaching around 65% of CeO^+ for 3 mm axial position. When using the 1.5 mm torch, the CeO^+ significantly increased when axial position was set below 5.0 mm, reaching up to 25% for 3 mm axial position. However, the torch equipped with a 2.5 mm injector with hTISIS operating at room temperature, provided a stable value of oxide ratio for the studied range. These observations agreed with the different kinetic energies of the ions in the plasma depending on the injector inner diameter. Narrower injectors provided an aerosol with higher kinetic energy, reducing the residence time of the ions in the plasma.

When the hTISIS temperature was increased up to 300 ºC, the differences between injectors showed the same trend. However, the oxide ratios for each torch increased for higher axial positions. For the 1.0 mm injector, the CeO^+ ratio increased from 10 to 3 mm, reaching at this axial position a value close to 90%. When the 1.5 mm injector was used, the ratio increased below 7.5 mm and this parameter reached up to 30% for a 3 mm axial position. Finally, when the 2.5 mm was used in combination with hTISIS at 300°C, the oxide ratio increased when the axial position was set below 5 mm, but in this case the CeO^+ ratio was lower than 2%, providing the best conditions in terms of oxide ratio. The observations made when hTISIS was heated at 300°C agreed with the solvent transport efficiency increase caused by heating the spray chamber walls, that increased the amount of oxygen in the central channel of the plasma. In previous studies carried out with the hTISIS, it was demonstrated that the transport efficiency was near 100% under these conditions.[21,40]

The CeO^+ radial profiles were also monitored when using the hTISIS at room temperature and at 300°C. For the 1.0 mm and 1.5 mm injectors, the work with the hTISIS at room temperature, yielded a maximum in the CeO^+ ratio at the plasma central channel for the three matrices studied, thus revealing the plasma thermal degradation caused by the solvent reaching it at relative high kinetic energy. When hTISIS was heated up to 300°C, the thermal degradation was more obvious, providing higher values of CeO^+ ratio. However, for the 2.5 mm injector, the CeO^+ ratio remained almost stable in the region from -1.0 to 1.0 mm, indicating that a more homogeneous plasma in terms of thermal stability was obtained and it was not significantly affected by the hTISIS temperature.

The Ce^{++} ratio did not present clear trends depending on the plasma sampling zone. The Ce^{++} ratio was in between 0.5 and 5% depending on the matrix and hTISIS temperature, showing moderate values as compared to CeO^{+} ratios, which reached values up to 90%. The hTISIS temperature did not significantly change the Ce^{++} ratios, obtaining similar ratios and trends when the same injector was studied under different hTISIS temperatures. When different injectors were studied, the differences were more significant. For 2.5 mm injector, the maximum Ce^{++} ratio was obtained at axial position 5 mm, whereas this maximum was reached at axial positions 10 and 15 mm for 1.5 mm and 1.0 mm injectors, respectively. These maximum ratios were 2.8%, 3.6% and 5.0% for 2.5 mm, 1.5 mm and 1.0 mm injectors, respectively. However, further studies will be performed to clearly stablish the effect of the injector and plasma thermal state on the Ce^{++} ratio, since the mass bias and ion repulsion in the interface need to be also studied.

The $^{36}Ar^{+}$ intensity was also monitored for different sampling positions, the three injectors studied and the hTISIS operated both at room temperature and 300ºC (Figure 6.b). This parameter is also an indicator of the plasma thermal state. The general trends were in agreement with those observed for CeO^{+} ratio. The $^{36}Ar^{+}$ signal increased as the injector diameter went up, thus providing a more robust plasma. Additionally, the 2.5 mm injector afforded an almost flat curve from 10 to 20 mm even when the hTISIS was heated at 300°C, indicating the good plasma thermal stability when working under these conditions. When the injectors with inner diameters of 1.5 mm and 1.0 mm were used, the $^{36}Ar^{+}$ intensity profile showed a peak at 19 mm and 22 mm axial position, respectively.

View Article Online
DOI: 10.1039/D1JA00134E

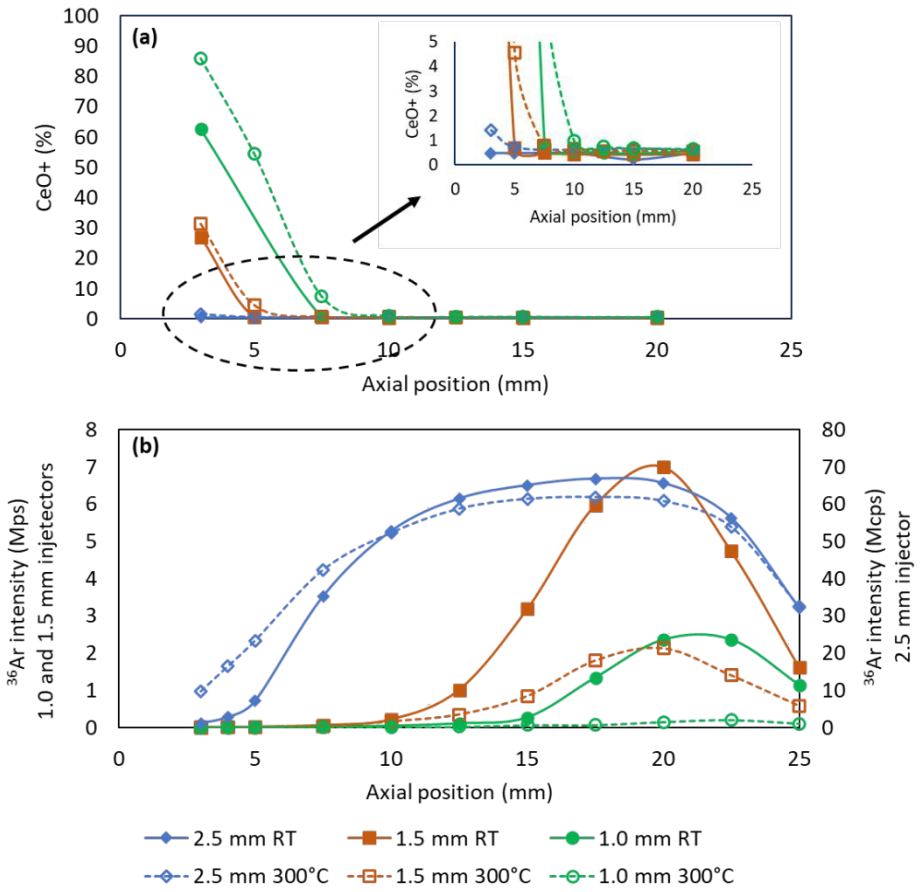

Figure 6. Axial profiles of (a) CeO^+ (%) and (b) $^{36}Ar^+$ for the three injectors studied in the present work at room temperature and 300°C. Matrix: 25% ethanol. Radial position: 0.0 mm. Extraction lens 1 and 2 at 0V and -200V, respectively. Rest of parameters: See Table 1.

Analysis of real samples.

The analysis of twenty alcoholic real samples (bioethanol and spirit beverages) was performed taking the ionic intensities at different regions of the plasma (*i.e.* different sampling zones) to demonstrate the application of the above drawn conclusions regarding matrix effects (see section "Matrix effects caused by ethanol"). Two sets of

View Article Online
DOI: 10.1039/D1JA00134E

calibration standards were prepared: (i) aqueous standards and (ii) 25% ethanol (v/v) matrix using external calibration and the hTISIS at 300 ^{o}C as a sample introduction system. Calibration curves obtained for both calibration sets were compared and not statistically differences were found. Thus, in order to simplify the discussion, only the results obtained by using the 25% ethanol standards have been included.

In order to check the extent of the matrix effects previously shown in this work, five different regions of the plasma were studied by modifying the axial and radial positions. Figure 7 shows the mean recoveries obtained for As (Figure 7.a), Cd (Figure 7.b), Co (Figure 7.c) and Ni (Figure 7.d) for twenty samples spiked at 100 ng mL^{-1} with the analytes gathered in Table 1. The recoveries were calculated by means of the difference between the spiked and non-spiked samples. In all cases, the mean recovery was close to 100%. However, the dispersion of the results was completely different depending on the region of the plasma sampled. When those samples were analyzed under sampling positions where it has been demonstrated that matrix effects caused by ethanol content were significant, several samples provided recoveries far away from 100%. The plasma sampling zone where matrix effects were most significant corresponded to 10 mm axial position and 0.0 mm radial position, which was the default position for aqueous mode routine analysis. Under these conditions, the recoveries obtained for the twenty samples ranged from 30% to 130%. However, when the same spiked samples were analyzed under optimum conditions in terms of matrix effects (*i.e.,* axial position: 10 mm, radial position: -1.0 mm, see Figure 5.a), the recoveries for all the samples and analytes were between 80 and 115%, demonstrating that matrix effects were completely removed. It is important to note that under these conditions, RSD values were around 10%. According to Figure 5.b, matrix effects could also be removed for a 3

View Article Online
DOI: 10.1039/D1JA00134E

mm and 0.0 mm axial and radial positions, respectively (Figure 7.b for Cd, Figure 7.c, for Co and Figure 7.d, for Ni). Nevertheless, As (Figure 7.a) showed a different behavior at this plasma sampling region, providing recoveries up to 170%. This increase on As recovery was probably caused by the polyatomic interference by $^{40}Ar^{35}Cl^{+}$ that can affect the results even when He mode is being used. This observation agreed with the trends observed for oxide ions (Figure 6.a).

This study highlights those results regarding matrix effects caused by ethanol, and its dependence on the plasma sampled zone, previously discussed (Figure 5) can be applied to the analysis of real samples.

Table 2 shows the found analyte concentrations for a set of twelve analytes in twenty real samples of bioethanol diluted 1:1 (v/v) with ultrapure water (six hydrated and non-hydrated bioethanol samples obtained from different raw materials) and non-diluted spirit beverages containing between 11 and 40% of ethanol (two vodka, three gyn, three whiskey, one rum, one apple liqueur, two white wines and two red wines). Distilled samples presented concentrations below the limit of quantification (LOQ) for almost all the analytes whereas wine samples, both red and white, presented relative high concentrations of several analytes, such as Mn, Fe, Zn, Rb and Sr.[3,7] These analytes and ranges of concentrations have been already reported by other authors in previous studies. Additionally, the apple liqueur appeared to be the spirit beverage with the highest concentrations of Fe and Cu. In the case of whiskey, Cu was found at moderate concentrations. This element could be considered as a good indicator of the whiskey production procedure because, traditionally, copper pot stills have been employed for the distillation.[41]

View Article Online
DOI: 10.1039/D1JA00134E

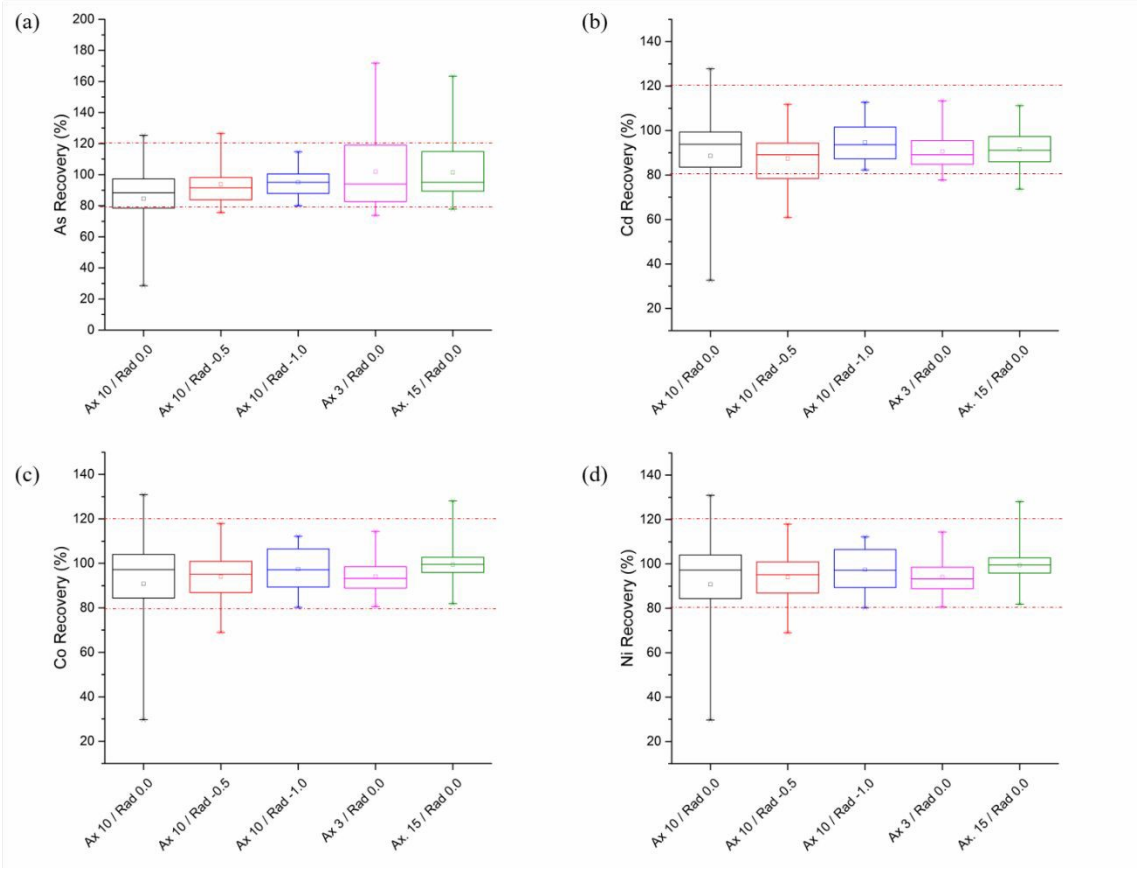

Figure 7. Recoveries obtained for twenty alcoholic beverages and bioethanol samples analyzed with hTISIS at 300°C in five different sampling positions. (a) As; (b) Cd; (c) Co; and (d) Ni. Calibration standards prepared in 25% ethanol. Ax: horizontal plasma sampling position; Rad: vertical plasma sampling position.

Table 2. Analyte concentration (ng mL^{-1}) found in 20 real samples (bioethanol, wines, and spirit beverages) measured under optimum conditions in terms of matrix effects (axial position: 10 mm, radial position: -1.0 mm). Confidence levels for n=3 and α=0.05. LOQ values are given in brackets.

Sample	V	Cr	Mn	Fe	Co	Ni	Cu	Zn	As	Rb	Sr	Cd
Bioethanol 1	11.3 ± 0.9	< LOQ (1.4)	3.30 ± 0.12	1.77 ± 0.19	0.58 ± 0.12	< LOQ (1.2)	< LOQ (2)	< LOQ (1.7)	< LOQ (0.4)	< LOQ (0.3)	< LOQ (1.5)	< LOQ (0.4)
Bioethanol 2	1.86 ± 0.03	1.9 ± 0.5	0.79 ± 0.09	< LOQ (0.7)	< LOQ (0.2)	< LOQ (1.2)	< LOQ (2)	< LOQ (1.7)	< LOQ (0.4)	< LOQ (0.3)	< LOQ (1.5)	< LOQ (0.4)
Bioethanol 3	< LOQ (0.2)	< LOQ (1.4)	< LOQ (0.5)	< LOQ (0.7)	< LOQ (0.2)	< LOQ (1.2)	< LOQ (2)	< LOQ (1.7)	< LOQ (0.4)	< LOQ (0.3)	< LOQ (1.5)	< LOQ (0.4)
Bioethanol 4	< LOQ (0.2)	< LOQ (1.4)	1.05 ± 0.04	< LOQ (0.7)	< LOQ (0.2)	< LOQ (1.2)	< LOQ (2)	< LOQ (1.7)	< LOQ (0.4)	< LOQ (0.3)	< LOQ (1.5)	< LOQ (0.4)
Bioethanol 5	< LOQ (0.2)	< LOQ (1.4)	< LOQ (0.5)	< LOQ (0.7)	< LOQ (0.2)	< LOQ (1.2)	< LOQ (2)	< LOQ (1.7)	< LOQ (0.4)	< LOQ (0.3)	< LOQ (1.5)	< LOQ (0.4)
Bioethanol 6	4.84 ± 0.18	< LOQ (1.4)	< LOQ (0.5)	< LOQ (0.7)	< LOQ (0.2)	< LOQ (1.2)	< LOQ (2)	< LOQ (1.7)	< LOQ (0.4)	< LOQ (0.3)	< LOQ (1.5)	< LOQ (0.4)

Vodka 1	4.7 ± 0.4	< LOQ (1.4)	< LOQ (0.5)	13.2 ± 0.4	< LOQ (0.2)	< LOQ (1.2)	< LOQ (2)	< LOQ (1.7)	< LOQ (0.4)	< LOQ (0.3)	< LOQ (1.5)	< LOQ (0.4)
Vodka 2	3.1 ± 0.7	< LOQ (1.4)	< LOQ (0.5)	< LOQ (0.7)	< LOQ (0.2)	< LOQ (1.2)	< LOQ (2)	< LOQ (1.7)	< LOQ (0.4)	< LOQ (0.3)	< LOQ (1.5)	< LOQ (0.4)
Gin 1	1.33 ± 0.15	< LOQ (1.4)	< LOQ (0.5)	2.7 ± 0.7	< LOQ (0.2)	< LOQ (1.2)	< LOQ (2)	< LOQ (1.7)	< LOQ (0.4)	< LOQ (0.3)	< LOQ (1.5)	< LOQ (0.4)
Gin 2	12 ± 2	0.92 ± 0.16	< LOQ (0.5)	3.3 ± 0.2	< LOQ (0.2)	< LOQ (1.2)	< LOQ (2)	< LOQ (1.7)	< LOQ (0.4)	< LOQ (0.3)	< LOQ (1.5)	< LOQ (0.4)
Gin 3 (Rose)	0.51 ± 0.14	< LOQ (1.4)	< LOQ (0.5)	4.1 ± 0.9	< LOQ (0.2)	< LOQ (1.2)	3.3 ± 0.2	< LOQ (1.7)	7.2 ± 0.6	1.12 ± 0.11	< LOQ (1.5)	< LOQ (0.4)
Whiskey 1	1.9 ± 0.3	< LOQ (1.4)	< LOQ (0.5)	< LOQ (0.7)	< LOQ (0.2)	< LOQ (1.2)	< LOQ (2)	< LOQ (1.7)	< LOQ (0.4)	< LOQ (0.3)	< LOQ (1.5)	< LOQ (0.4)
Whiskey 2	2.9 ± 0.4	1.4 ± 0.3	12.7 ± 0.7	71 ± 7	0.83 ± 0.15	< LOQ (1.2)	110 ± 7	< LOQ (1.7)	< LOQ (0.4)	8.0 ± 0.5	12.2 ± 1.5	< LOQ (0.4)
Whiskey 3	0.92 ± 0.03	6.0 ± 1.0	16.6 ± 0.2	30 ± 3	< LOQ (0.2)	< LOQ (1.2)	157 ± 5	< LOQ (1.7)	< LOQ (0.4)	8.0 ± 1.0	2.0 ± 0.3	< LOQ (0.4)

Apple liqueur 1	14.2 ± 1.1	1.5 ± 0.3	7.7 ± 1.3	101 ± 6	1.03 ± 0.05	< LOQ (1.2)	346 ± 18	17.0 ± 1.5	44.9 ± 0.2	< LOQ (0.3)	10.2 ± 0.7	1.4 ± 0.3
Rum 1	4.8 ± 0.7	< LOQ (1.4)	6.0 ± 0.3	55 ± 3	< LOQ (0.2)	< LOQ (1.2)	25 ± 2	< LOQ (1.7)	11.7 ± 0.6	4.7 ± 0.2	2.0 ± 0.3	< LOQ (0.4)
White wine 1	22.4 ± 1.3	4.9 ± 0.9	659 ± 40	904 ± 59	2.5 ± 0.3	9.2 ± 0.8	28.6 ± 1.6	330 ± 33	18.3 ± 0.6	490 ± 41	512 ± 50	1.10 0.08
White wine 2	57.1 ± 0.6	8.2 ± 1.0	629 ± 42	522 ± 42	1.57 ± 0.06	7.5 ± 0.9	31 ± 3	275 ± 10	15.6 ± 0.8	1140 ± 99	322 ± 36	< LOQ (0.4)
Red wine 1	3.7 ± 0.4	4.1 ± 0.8	717 ± 47	1279 ± 127	2.13 ± 0.08	8.3 ± 0.9	27 ± 2	292 ± 12	12.8 ± 0.9	379 ± 17	1030 ± 110	< LOQ (0.4)
Red wine 2	1.26 ± 0.13	6.6 ± 1.0	580 ± 38	1291 ± 85	1.10 ± 0.15	7.8 ± 1.7	32 ± 3	361 ± 16	10.3 ± 1.1	465 ± 28	801 ± 52	< LOQ (0.4)

Conclusions

The use of the hTISIS for the direct bioethanol, wine and spirit beverages elemental analysis through ICP-MS equipped with a HMI device provides accurate results without the need for the addition of an oxygen additional stream. Thanks to the high temperatures of the sample introduction system, 100% analyte transport efficiency was reached irrespectively of the matrix sample, thus allowing external calibration based on the use of ethanol:water (1:4 v/v) standards. Furthermore, the ICP-MS sensitivity achieved under these conditions is high enough to perform trace elemental analysis.

Moreover, as it was previously demonstrated,[21] in order to improve the accuracy of the determination, it is necessary to deeply study the spatial distribution of ion cloud in the ICP-MS plasma. The obtained results demonstrated that taking the ionic signal at the plasma central channel did not provide accurate results. Furthermore, the optimum plasma sampling zone in terms of matrix effects did not match with that in terms of sensitivity. Therefore, in order to achieve reliable data, it is mandatory to perform the optimization of the instrument in terms of lack of interferences rather than in terms of ionic counting.

By carefully selecting the right conditions for both aerosol transport, analyte ionization and plasma ion sampling as well as ion transmission, it is possible to achieve suitable data without the need for an auxiliary technique such internal standardization. If required, an IS could be added to further improve the precision of the method. This fact makes ICP-MS to be considered as a robust routine analysis technique.

Conflicts of interest

There are no conflicts to declare.

Acknowledgements

The authors wish to thank the Spanish Ministry of Science, Innovation and Universities for the financial support (Project Ref. PGC2018-100711-B-I00). Authors would also like to thank IFPEn for the financial support. C. Sánchez thanks to the Ministry of Education, Spain for the contract FPU 13/01438.

References

1 J.G. Ibañez, A. Carreón-Álvarez, M. Barcena-Soto and N. Casillas, *J. Food Compos. Anal.*, 2008, **21**, 672-683.

2 P. Pohl, *Trends Anal. Chem.*, 2007, **26**, 941-949.

3 S.M. Rodrigues, M. Otero, A.A. Alves, J. Coimbra, M.A. Coimbra, E. Pereira and A.C. Duarte, *Food. Compos. Anal.*, 2011, **24**, 548-562.

4 H. Mayer, O. Marconi, S. Floridi, L. Montanari and P. Fantozzi, *J. Inst. Brew.*, 2003, **109**, 332-336.

5 P.J.S. Barbeira and N.R. Stradiotto, *Fresenius J. Anal. Chem.*, 1998, **361**, 507-509.

6 A. Bica, R. Sánchez and J.L. Todolí, *Molecules*, 2020, **25**, 2961-2978.

7 C. Ceruti, C. Sánchez, R. Sánchez, F. Ardini, M. Grotti and J.L. Todolí, *J. Anal. At. Spectrom.*, 2019, **34**, 674-682

8 R. Sánchez, C. Sánchez, C.P. Lienemann and J.L. Todolí, *J. Anal. At. Spectrom.*, 2015, **30**, 64–101.

View Article Online
DOI: 10.1039/D1JA00134E

9 H. Habe, T. Shinbo, T. Yamamoto, S. Sato, H. Shimada and K. Sakaki, *J. Japan Pet. Inst.*, 2013, **56**, 414–422.

10 C. C. Leite, A. de Jesus, M. L. Potes, M. A. Vieira, D. Samios and M. M. Silva, *Energy & Fuels*, 2015, **29**, 7358–7363.

11 ASTM International, *ASTM D4806-16a, Standard Specification for Denatured Fuel Ethanol for Blending with Gasolines for Use as Automotive Spark-Ignition Engine Fuel*, West Conshohocken, 2016.

12 ABNT - Associação Brasileira de Normas Técnicas, *ABNT NBR 11331- Ethyl alcohol – Determination of iron and copper concentrations – Atomic absorption spectrophotometry method*, 2007.

13 C. Sánchez, S. Santos, R. Sánchez, C.P. Lienemann and J.L. Todolí, ACS Omega, 2020, **5**, 20912–20921.

14 C. Sánchez, C.P. Lienemann and J.L. Todolí, *Spectrochim. Acta Part B At. Spectrosc.*, 2016, **115**, 16–22.

15 R. S. Amais, G. L. Donati, D. Schiavo and J. A. Nóbrega, *Microchem. J.*, 2013, **106**, 318–322.

16 E. McCurdy and D. Potter, *Agil. Technol.*, 2002, **1**, 5988-6190E.

17 D.R. Neves, R.S. Amais, J.A. Nóbrega and J.A.G. Neto, *Anal. Lett.*, 2012, **45**¸1111-1121.

18 M.S. Rocha, M.F. Mesko, F.F. Silva, R.C. Sena, M.C.B. Quaresma, T.O. Araújo and L.A. Reis, *J. Anal. At. Spectrom.*, 2011, **26**, 456-461.

19 C. Sánchez, J.P. Vidal, C.P. Lienemann and J.L. Todolí, *Fuel Process. Technol.*, 2018, **173**, 1-10.

View Article Online
DOI: 10.1039/D1JA00134E

20 C. Ekberg, P.L. Brown, A. Odegaard-Jensen, D.M. Hill and A.W. Zawadzki, *Anal. Bioanal. Chem.*, 2002, **374**, 1330-1334.

21 C. Sánchez, C.P. Lienemann and J.L. Todolí, *Spectrochim. Acta Part B At. Spectrosc.*, 2016, **124**, 99-108.

22 A. E. Holliday and D. Beauchemin, *Spectrochim. Acta - Part B At. Spectrosc.*, 2004, **59**, 291–311.

23 A. L. Gray and A. R. Date, *Analyst*, 1983, **108**, 1033–1050.

24 E. Poussel, J.M. Mermet and D. Deruaz, *J. Anal. At. Spectrom.*, 1994, **9**, 61–66.

25 G. Horlick, S. H. Tan, M. A. Vaughan and C. A. Rose, *Spectrochim. Acta Part B At. Spectrosc.*, 1985, **40**, 1555–1572.

26 M.A. Vaughan, G. Horlick and S. H. Tan, *J. Anal. At. Spectrom.*, 1987, **2**, 765-772.

27 B.S. Ross, D.M. Chambers, G.H. Vickers, P. Yang and G.M. Hieftje, *J. Anal. At. Spectrom.*, 1990, **5**, 351–358.

28 S. Liu and D. Beauchemin, *Spectrochim. Acta - Part B At. Spectrosc.*, 2006, **61**, 157–163.

29 N. Jakubowski, I. Feldmann and D. Stuewer, *Spectrochim. Acta Part B At. Spectrosc.*, 1992, **47**, 107–118.

30 M.P. Dziewatkoski, L.B. Daniels and J.W. Olesik, *Anal. Chem.*, 1996, **68**, 1101–1109.

31 G. Zhu and R. F. Browner, *Appl. Spectrosc.*, 1987, **41**, 349–359.

32 L. A. Norman, M. Muñoz, D. P. Myers, B. S. Ross and G. M. Hieftje, *Appl. Spectrosc.*, 1992, **46**, 448–457.

33 M. Aghaei, L. Flamigni, H. Lindner, D. Günther and A. Bogaerts, *J. Anal. At. Spectrom.*, 2014, **29**, 249-261.

View Article Online
DOI: 10.1039/D1JA00134E

34 D. C. Gregoire, *Spectrochim. Acta Part B At. Spectrosc.*, 1987, **42**, 895–907.

35 M. Aghaei, H. Lindner and A. Bogaerts, *Spectrochim. Acta - Part B At. Spectrosc.*, 2012, **76**, 56–64.

36 H. Lindner, A. Murtazin, S. Groh, K. Niemax and A. Bogaerts, *Anal. Chem.*, 2011, **83**, 9260–9266.

37 M. Aghaei, H. Lindner and A. Bogaerts, *J. Anal. At. Spectrom.*, 2013, **28**, 1485–1492.

38 R. Sánchez, C. Sánchez, J.L. Todolí, C.P. Lienemann and J.M. Mermet, *J. Anal. At. Spectrom.*, 2014, **29**, 242–248.

39 Y. Makonnen and D. Beauchemin, *Spectrochim. Acta - Part B At. Spectrosc.*, 2015, **103-104**, 57-62.

40 R. Sánchez, J.L. Todolí, C.P. Lienemann and J.M. Mermet, J. Anal. At. Spectrom., 2012, 27, 937-945.

41 T. Adam, E. Duthie and J. Feldmann, *J. Inst. Brew.*, 2002, **108**, 459-464.